Supporting Online Material for:

Self-Assembly of Giant Peptide Nanobelts

Honggang Cui, Takahiro Muraoka, Andrew Cheetham, Samuel I. Stupp

Department of Materials Science and Engineering, Department of Chemistry, and Feinberg School of Medicine, Northwestern University, 2220 Campus Drive, Evanston, Illinois 60208. Institute for BioNanotechnology in Medicine, Northwestern University, Chicago, IL 60611

E-mail: s-stupp@northwestern.edu

S1. Synthesis and Purification of peptide molecules

Peptides were synthesized using standard 9-fluorenylmethoxycarbonyl (Fmoc) solid phase peptide synthesis at 0.5 mmol scale. Fmoc deprotections were performed with 30% piperidine–DMF solution for 10 min. Cleavage of the peptides from the Wang resin was carried out with a mixture of trifluoroacetic acid (TFA)/triisopropylsilane (TIS)/H_2O in a ratio of 95/2.5/2.5 for 3 hours. Excess TFA was removed by rotary evaporation. The remaining peptide solution was triturated with cold diethyl ether and the precipitate was centrifuged, and the supernatant liquid was removed by decantation. After washing with diethyl ether (three times) to remove residual TFA, the precipitate was dried under vacuum overnight. The peptides were purified by preparative RP-HPLC using a Phenomenex Gemini column (C18, 10u, 100Å, 30X150mm) at 25 ºC on a VARIAN Prostar Model 210 preparative HPLC system. Water/acetonitrile gradient containing 0.1 vol % NH_4OH was used as an eluent at a flow rate of 25 mL min^{-1}. The purified fractions were collected and concentrated by rotary evaporation to remove acetonitrile, then lyophilized and stored at –20 ºC. The peptides were later characterized by electrospray ionization mass spectrometry (ESI-MS) using an Agilent 6510 quadrupole time-of-flight (Q-Tof) instrument, with 0.1% NH_4OH in a water-acetonitrile mix (70:30) as eluent. Reverse phase HPLC was performed on a Hewlett-Packard 1050 liquid chromatograph equipped with a Waters X-Bridge column (C18, 4.6 mm × 150 mm) in elution gradient of water (0.1% NH_4OH) and acetonitrile (0.1% NH_4OH).

S2. Characterization method of assembled nanostructures

Tapping mode atomic force microscopy (AFM) was performed on a MultimodeTM SPM equipped with a J scanner (Digital Instruments). Aged nanobelt solutions at a concentration of 0.1% (~2μL) were deposited onto freshly cleaned mica that was glued to a stainless steel sample disc. The samples were left to dry in a ventilation hood. These samples were imaged using silicon probes with aluminum reflex coating.

Cryogenic transmission electron microscopy (Cryo-TEM) imaging was performed on a JEOL 1230 microscope, operating at 80 kV. A small droplet of the solution (5-10 μL) was placed on a holey carbon film supported on a TEM copper grid within a controlled environment vitrification system (Gatan Inc.). The specimen was blotted and plunged into a liquid ethane reservoir cooled by liquid nitrogen. The vitrified samples were transferred to a Gatan 626 cryo-holder and cryo-transfer stage cooled by liquid nitrogen. During observation of the vitrified samples, the cryo-holder temperature was maintained below -170 °C to prevent sublimation of vitreous water. The images were recorded digitally with a CCD camera.

Staining-and-drying TEM samples were prepared as follows: a small volume (~5μl) of dilute solution was deposited onto a carbon-coated copper grid. The excess of the solution was quickly wicked away by a piece of filter paper. The sample was subsequently left to dry. Once dried, the samples were negatively stained by placing a drop of 2 wt% uranyl acetate aqueous solution on the top. A thin layer of uranyl acetate solution was left after blotting away excess of the uranyl acetate solution. Again, the samples were left to dry under ambient conditions. Bright-field TEM imaging of the

assembled structures was performed on a JEOL 1230 Transmission Electron Microscope, operating at 100kV.

Small angle neutron scattering (SANS) experiments were performed on the 30 m facility (NG3) at the National Institute of Standards and Technology (NIST) center for Cold Neutron Research (Gaithersburg, MD). All the experiments were conducted at ambient temperature. The neutron wavelength was $\lambda = 6$Å with a wavelength spread of $\Delta\lambda/\lambda = 0.15$. Sample solutions were loaded in 2 mm cells with quartz windows. Scattering data were collected at three sample-to-detector distances of 1.3, 4.0 and 13.1 m to obtain q value containing desired features in the scattering profile. The scattering wave vector is defined as $q = (4\pi/\lambda) \sin(\theta/2)$, where θ is the scattering angle. The two-dimensional data were corrected and averaged to one-dimensional data using data correction and reduction software developed by NIST scientists. The scattering intensities were scaled to absolute values on the basis of direct beam flux measurements.

S3a. Electrospray ionization mass spectrometry of $C_{16}H_{31}OVEVE$

i

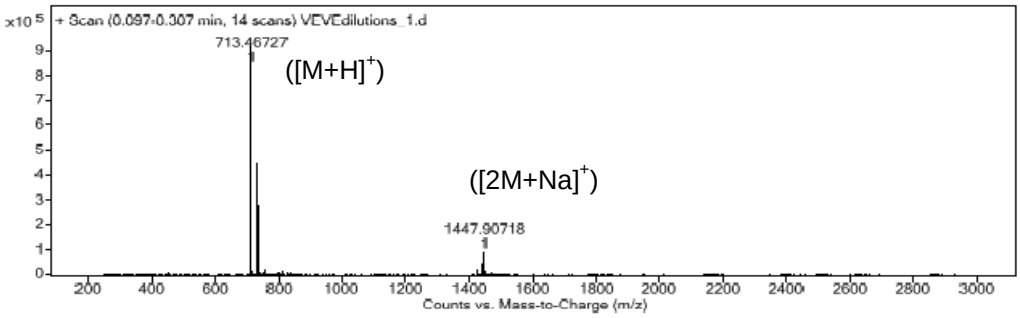

ii

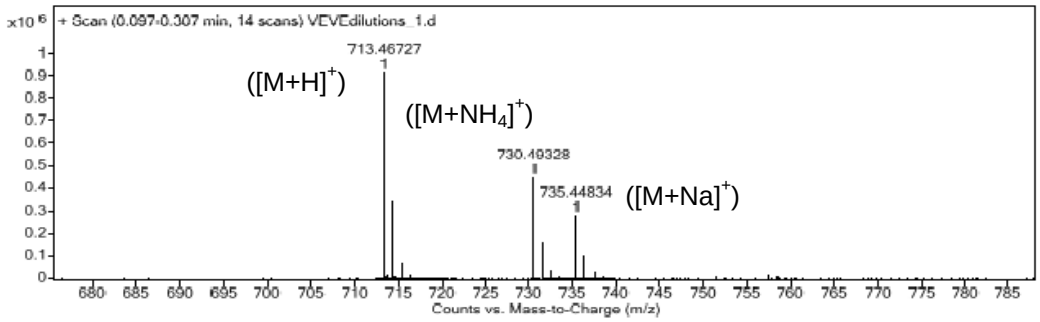

iii

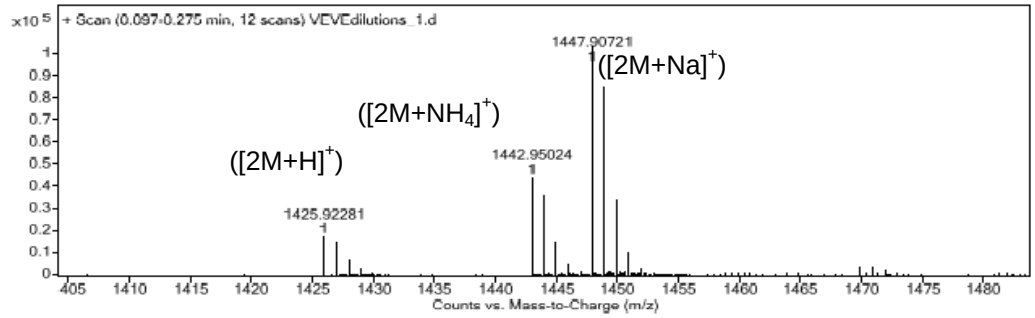

iv

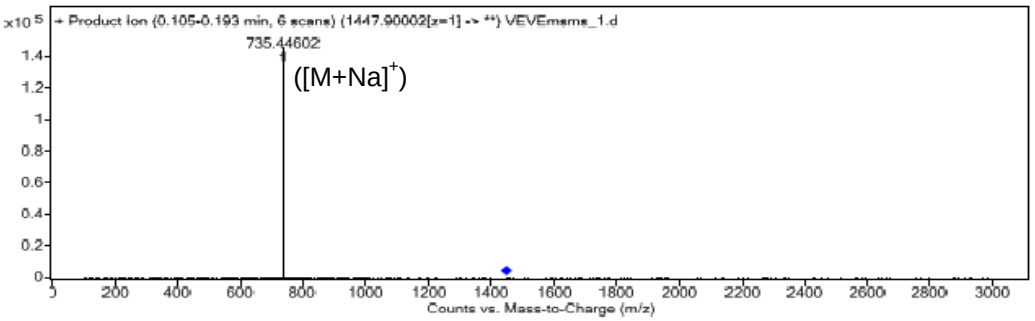

i) Full mass spectrum of $C_{16}H_{31}OVEVE$; ii) The expanded mass spectrum of the monomer peak; iii) The expanded mass spectrum of the dimer peak; iv) Tandem mass spectrum on the dimer peak. The protonated adduct of $C_{16}H_{31}OVEVE$ was observed at 713.47, as were the ammonium and sodium adducts, 730.19 and 735.45, respectively (Figure S3a(ii)). Also observed was the formation of a sodiated dimer, $[2M+Na]^+$, at 1447.91, and to a lesser extent the protonated and ammoniated forms at 1425.92 and

1442.95, respectively (Figure S3a(iii). The formation of a true dimer was confirmed by a tandem mass spectrometry experiment (or MS/MS) whereby the sodiated dimer was targeted for collision-induced dissociation (CID), resulting in its breaking apart to give the monomeric sodiated species $[M+Na]^+$ (Fig. S3a(iv)). The blue dot indicates which ion was selected for CID.

S3b. Electrospray ionization mass spectrometry of $C_{16}H_{31}$OVEVEGRGD

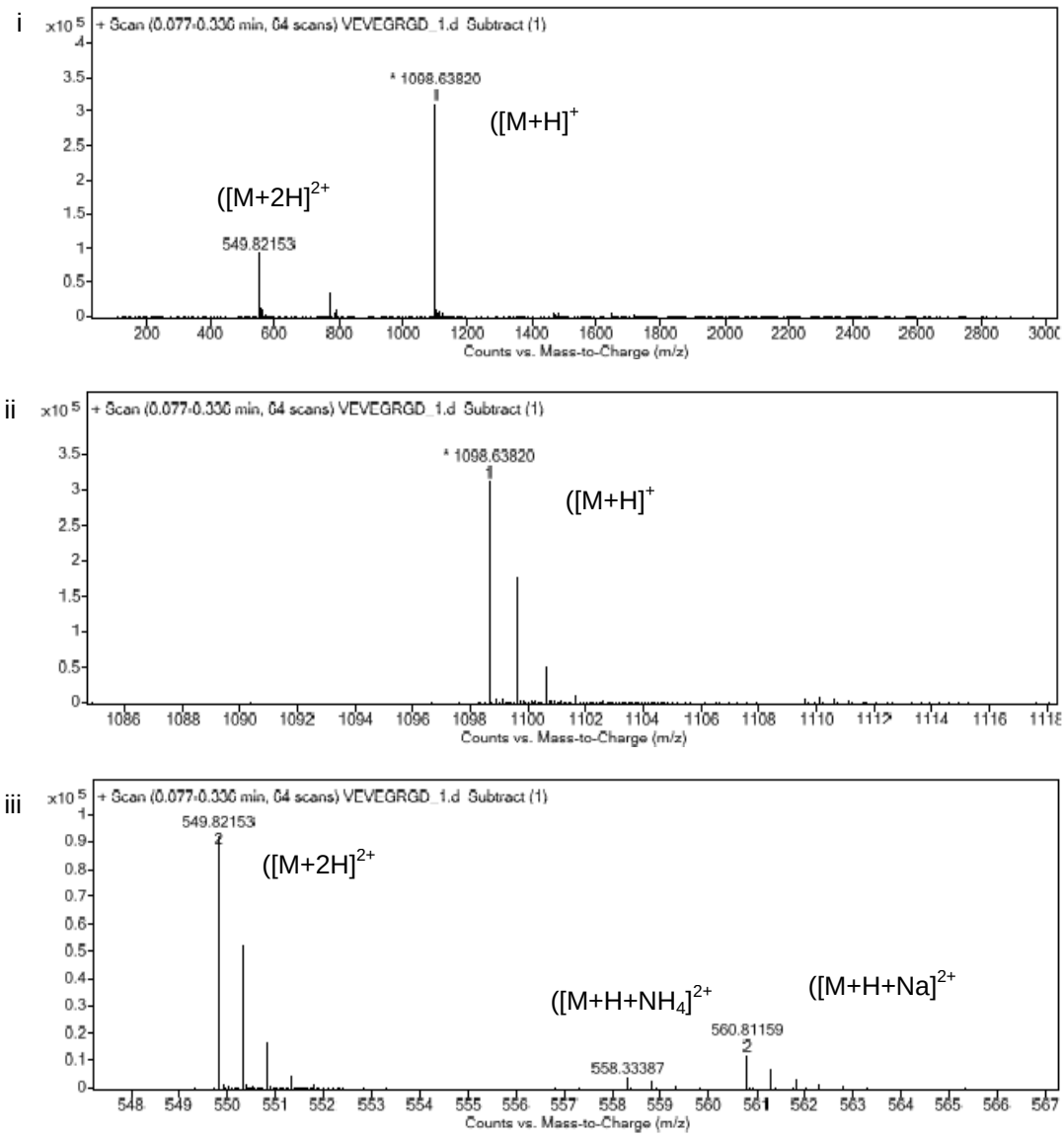

i) Full mass spectrum of $C_{16}H_{31}$OVEVEGRGD; ii) The expanded mass spectrum of the monomer peak; iii) The expanded mass spectrum of the monomer peak carrying two charges. The protonated adduct of $C_{16}H_{31}$OVEVE was observed at 1098.64 and 549.82, respectively.

S3c. Analytical Reverse-Phase HPLC of $C_{16}H_{31}OVEVE$

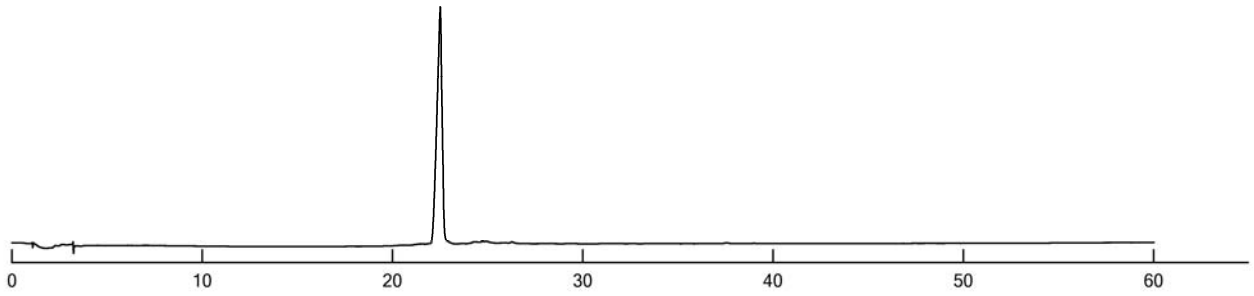

S3d. Analytical Reverse-Phase HPLC of $C_{16}H_{31}OVEVEGRGD$

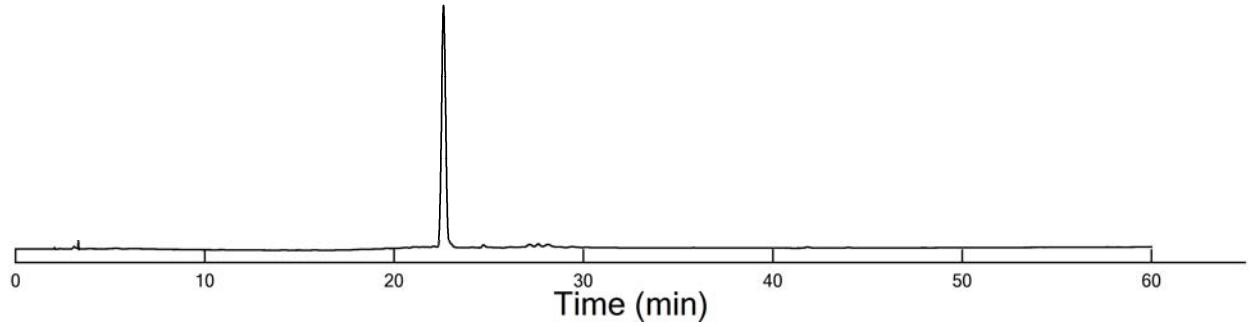

S4. Height measurement of nanobelts by AFM

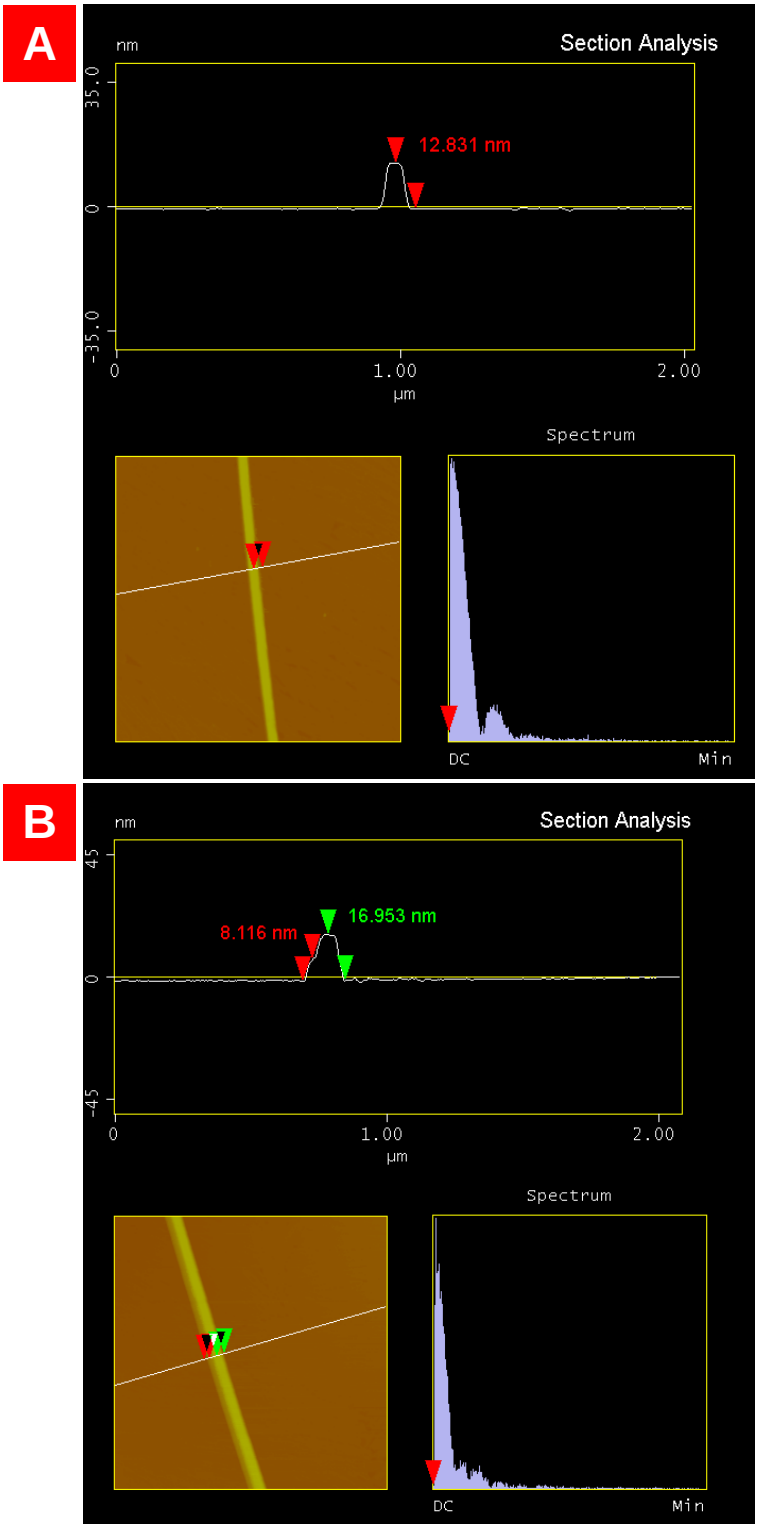

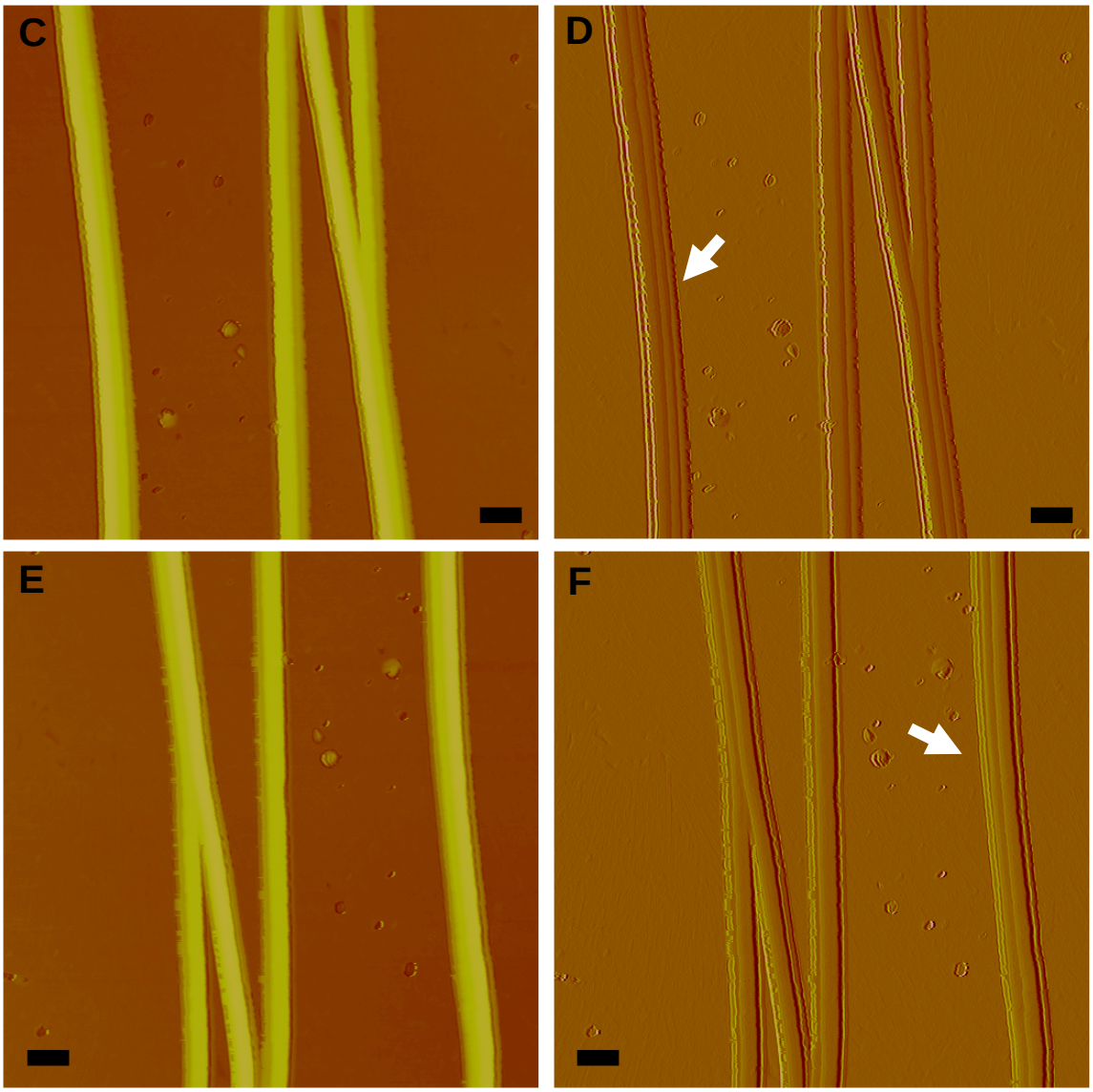

Fig. S4 A Nanobelt height measurement of Figure 1e, 12.82nm; **B** Nanobelt height measurement of Figure 1f. Green marker, 16.95nm, and red marker, 8.12nm; **C** AFM height image of nanobelts; **D** Corresponding amplitude image of **C; E** AFM height image of the nanobelts in **C** but scanned from 180 scanning angle; **F** Corresponding amplitude image of **E**. AFM tip scans from left to right in both **C** and **E**. All scale bars: 200nm.

Summary

The AFM measurements in both Fig. S4A and S4B reveal that the nanobelts at 0.1 wt % solution are not a single peptide bilayer. Rather, the nanobelt in fig. S4A seems to have three peptide bilayers (4.27nm in thickness per bilayer) and the nanobelt in fig.S4B has four bilayers sticking together (4.24 nm in thickness per bilayer). Both measurements are

in agreement with the expected thickness of one interdigitated peptide bilayer (4.7nm) and SANS measurement (4.3nm).

The multiple stacking of peptide bilayers can be directly displayed by AFM imaging as shown in Figs. S4C-F. the appearance of layered lines in completely reverse scanning directions reveals that these layered lines are not artifacts resulting from AFM imaging.

S5. Plots of small angle neutron scattering (SANS) profiles of nanobelt solutions

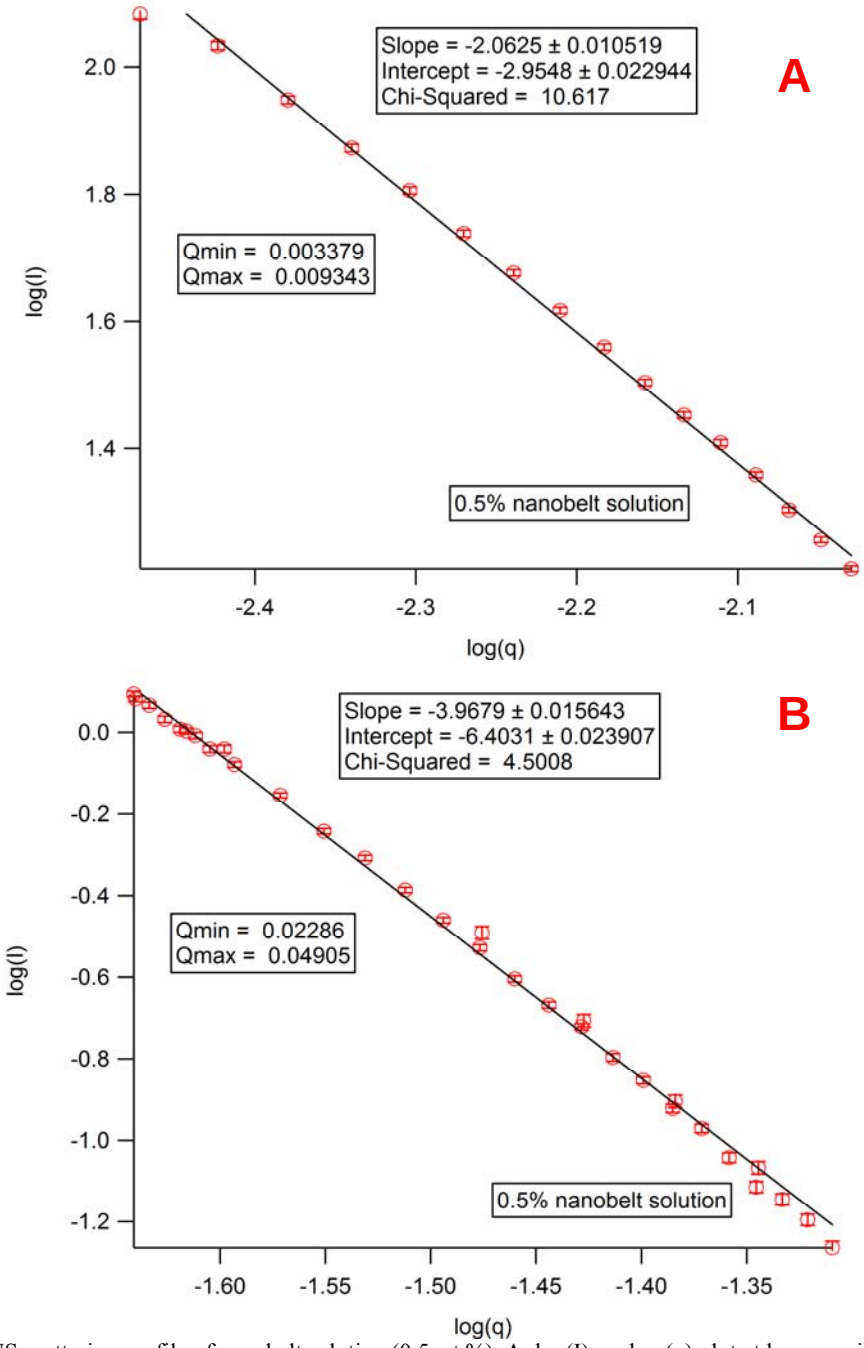

Fig. S5 SANS scattering profile of nanobelt solution (0.5 wt.%). A, log(I) vs. log (q) plot at low q region; B, log(I) vs. log (q) plot at high q region. The -2 scaling at low q indicates the flat shape of the nanobelt morphology. The -4 porod scaling suggests a sharp interface between the nanobelt and D_2O.

Using asymptotic expression, the form factor for a flat bilayer structure is given as follows:1

$$I(q) \approx 2\pi(\Delta\rho)^2 \varphi\delta / q^2 \propto q^{-2}$$

In which I(q) is the scattering intensity, q is the scattering wavevector, Δρ is the difference in scattering length desnsity, φ is the volume fraction, and δ is the bilayer thickness. This expression only applies at small q compared to transverse size δ (bilayer thickness).

A more accurate expression is given by Glatter and Kraky: 2

$$q^2 \bullet I(q) \approx 2\pi\varphi\delta(\Delta\rho)^2 \exp(-q^2\delta^2/12)$$

At small q limit,

$$\exp(-q^2\delta^2/12) \approx 1$$

Thus, we still have

$$I(q) \approx 2\pi(\Delta\rho)^2 \varphi\delta / q^2 \propto q^{-2}$$

1. Porte, G. *Neutrons, X-rays and Light: Scattering Methods Applied to Soft Condensed Matter* (eds. Lindner, P. & Zemb, T.) (Elsevier Science B.V., 2002).
2. Glatter, O. & Kratky, O. *Small Angle X-rays Scattering* (Academic Press, New York, 1982).

S6. Cryo-TEM image of $C_{16}H_{31}OVVEE$

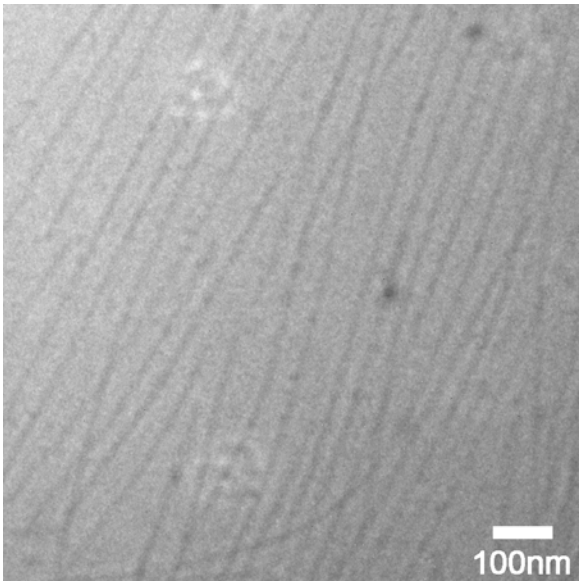

Figure S6 Cryo-TEM image of 0.1 wt % $C_{16}H_{31}OVVEE$ aqueous solution clearly demonstrates cylindrical nanofibers. We propose that the alternating sequence of amino acids allows more effective chain packing within the peptide region, leading to formation of the nanobelt morphology. When the alternating sequence of VEVE was replaced with VVEE, the cylindrical curvature was regained back as shown in this cryo-TEM image.

S7. Width statistics of nanobelts

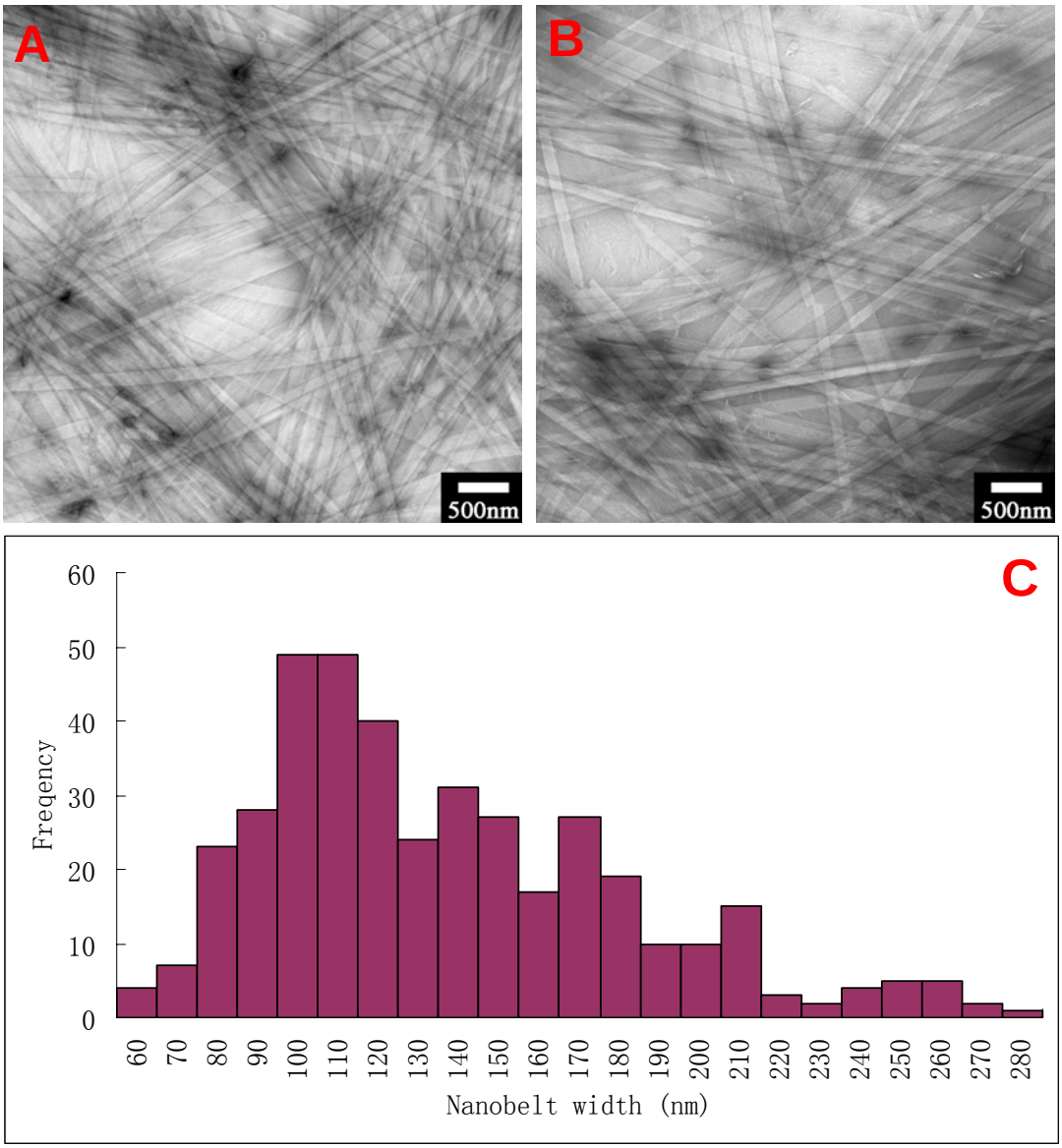

Fig. S7A-B TEM images of nanobelts in 0.1 wt % solution and **C** accompanying statistics of nanobelt widths (counted from 402 nanobelts). Most of the nanobelts have a width between 100nm and 150nm. The average nanobelt width is 141.6nm with a standard deviation of 44.3nm. The solution was aged for 4 months prior to TEM sample preparation and imaging.

S8. AFM measurement of grooved nanobelts at higher pH.

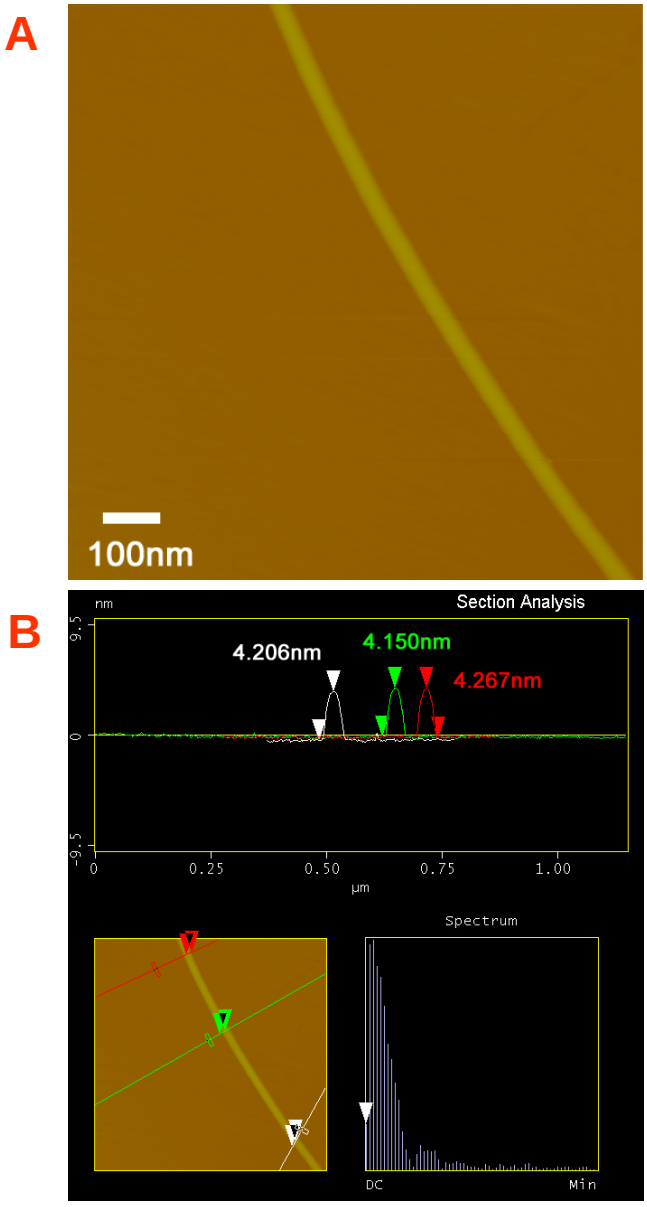

Figure S8 AFM measurement of grooved nanobelts at higher pH (2mM NaOH). **A** AFM height image of grooved nanobelts with a width of approximately 50 nm; **B** Section analysis of the nanobelt. Height measurements at three different locations were made, giving rise to 4.21 nm, 4.15 nm and 4.27 nm, respectively. These results indicates that the nanobelts formed at higher pH are single interdigitated bilayers, lacking stacking along the z-direction.